Supplementary Notes - Defect engineering of silicon with ion pulses from laser acceleration

Walid Redjem[1], Ariel J. Amsellem[2], Frances I. Allen[3, 4], Gabriele Benndorf[5], Jianhui Bin[2,6], Stepan Bulanov[2], Eric Esarey[2], Leonard C. Feldman[7], Javier Ferrer Fernandez[8, 9], Javier Garcia Lopez[8, 9], Laura Geulig[2, 11], Cameron R. Geddes[2], Hussein Hijazi[7], Qing Ji[2], Vsevolod Ivanov[2, 10], Boubacar Kante[1,2], Anthony Gonsalves[2], Jan Meijer[5], Kei Nakamura[2], Arun Persaud[2], Ian Pong[2], Lieselotte Obst-Huebl[2], Peter A. Seidl[2], Jacopo Simoni[9], Carl Schroeder[2, 12], Sven Steinke[2, 13], Liang Z. Tan, Ralf Wunderlich[5], Brian Wynne[2], and Thomas Schenkel[2,]*

[1]Department of Electrical Engineering and Computer Science, University of California, Berkeley, CA 94720, USA

[2]Accelerator Technology and Applied Physics Division, Lawrence Berkeley National Laboratory, Berkeley, CA 94720, USA

[3]Department of Materials Science and Engineering, University of California, Berkeley, CA 94720, USA

[4]California Institute for Quantitative Biosciences, University of California, Berkeley, CA 94720, USA

[5]Felix Bloch Institute for Solid State Physics, University Leipzig, Linnéstr. 5, D-04103 Leipzig, Germany

[6]present address: State Key Laboratory of High Field Laser Physics and CAS Center for Excellence in Ultra-Intense Laser Science, Shanghai Institute of Optics and Fine Mechanics, Chinese Academy of Sciences, Shanghai 201800, China

[7]Rutgers University, Department of Physics & Astronomy, 136 Frelinghuysen Rd, Piscataway, NJ 08854, USA

[8]Centro Nacional de Aceleradores, Universidad de Sevilla, CSIC and Junta de Andalucía, 41092 Sevilla, Spain

[9]Departamento de Física Atómica, Molecular y Nuclear, Universidad de Sevilla, 41012 Sevilla, Spain

[10]Molecular Foundry, Lawrence Berkeley National Laboratory, Berkeley, CA 94720, USA

[11]present address: Fakultät für Physik, Ludwig-Maximilians-Universität München, Am Coulombwall 1, 85748 Garching, Germany

[12]Department of Nuclear Engineering, University of California, Berkeley, CA 94720, USA

[13]Present address: Marvel Fusion GmbH, Blumenstrasse 28, D-80331 Munich, Germany

*corresponding author: T_Schenkel@LBL.gov

Supplementary Note 1. Time lapse movie showing evaporation of the aluminum foil mask during 100 shots.

Supplementary Note 2. Photoluminescence (PL) and Secondary Ion Mass Spectrometry (SIMS) data correlation to PL data

Supplementary Note 3. Details on energy deposition and heat calculations

Supplementary Note 4. Details on Nuclear Reaction Analysis (NRA)

Supplementary Note 5. Details on channeling Rutherford Backscattering (ch-RBS)

Supplementary Note 6. Supplemental material on Density Functional Theory (DFT) calculations of G and W-centers in silicon

Supplementary Note 1. Time lapse movie showing evaporation of the aluminum foil mask during 100 shots

Supplementary Figure 1: **Frames from a time lapse movie showing evaporation of the aluminum foil mask during 100 shots.** Frames from a movie (posted online) compiled from video camera images taken during a series of 100 shots at the BELLA PW laser where laser-accelerated protons and ions irradiated a silicon sample that was covered with aluminum foil (Figure 1, setup in main text). The real time repetition rate was 0.2 Hz. The film shows the gradual evaporation of the aluminum foil around the central aperture with an initial diameter of 5 mm. Link to the movie: https://www.youtube.com/watch?app=desktop&v=1Lxy5yUgQQY&feature=youtu.be

Supplementary Note 2. Photoluminescence spectra of photon emitting defects and SIMS depth profiles at the same locations

In Supplementary Figure 2, we complement the PL results from Figure 8 in the main text with SIMS depth profiles of carbon, oxygen and hydrogen of a sample that had received two laser-ion pulses. The SIMS depth profiles were taken in the same areas on the sample where PL spectra had been taken earlier. We observe G-centers from proton irradiation in areas just outside the central beam spot area that had been covered with aluminum foil, a). In areas with increased carbon concentrations we see W-centers with a narrow linewidth distribution and G-centers with a broadened distribution, b). Areas with the highest thermal budget and ion flux show W-center ensembles with a slightly broadened linewidth, c). The shape of the SIMS profile from the high flux area (c) is indicative of surface roughness increases due to the onset of exfoliation.

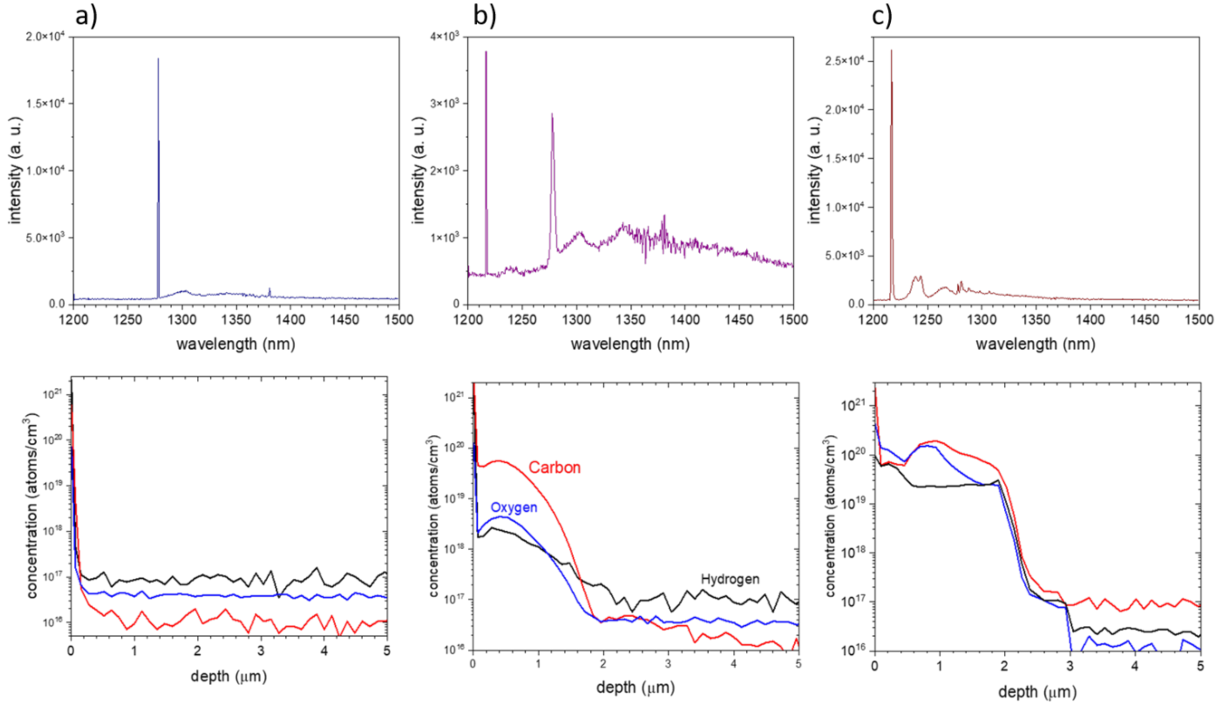

Supplementary Figure 2: **Photoluminescence (PL) and Secondary Ion Mass Spectrometry (SIMS) results from a silicon (111) sample after two laser ion pulses**. The PL spectra were taken first and SIMS depth profiles were then taken afterwards in the same locations. a) Narrow G-centers in areas with proton irradiation only (covered with Al foil), b) narrow W and broadened G-center from areas with increase carbon drive in diffusion and MeV carbon and proton flux, c) slightly broadened W-centers in areas with the highest energy deposition from laser ion pulses. SIMS depth profiles: carbon (red), oxygen (blue), hydrogen (black).

Supplementary Note 3. Details on energy deposition and heat calculations

In order to produce the temperature profiles shown in Figure 4 (main text), we time evolved a rectangular 2D region on the silicon sample using the heat diffusion equation. The initial temperature versus depth profiles for this region were derived from the measured SIMS ion concentrations versus depths. The ion concentrations were converted to temperature via the following scaling

$$\overrightarrow{T_0} = \frac{ions}{cm^3} \cdot \frac{1}{C_p \rho} \cdot \vec{E}$$

where $\vec{E}$ is an array of ion energies (interpolated from the SIMS depth via a SRIM table for carbon ions in silicon) and $\overrightarrow{T_0}$ is a vector of initial temperatures over the spot depth. As reported above, this conversion produced an unrealistically high local temperature, which — when extrapolated over the entirety of the sample irradiated by the ion pulse — would approach or exceed the total energy of the laser pulse that was focused into the foil targets at the given transmission of the laser focusing optics (~22 J of 39 J at a transmission of the laser optics of ~0.56). We consider two possible explanations for the enhanced carbon concentration at shallow depth: 1) The measured temperature enhancement

results from low energy carbon ions and particles from plasma expansion that reach a pre-heated surface and then rapidly diffusing into the sample in a manner similar to the diffusion of oxygen from the laser annealing of silicon with ~150–200 ns laser pulses [1]. 2) Since each SIMS spot only covers 100 μm^2, we may only be observing some small regions where the sample becomes exceedingly hot while others are much colder. This effect would be attributed to the fact that the beam is filamented and comprised of multiple high-intensity jets of ions. Hence, extrapolating locally very high energy deposition values from our SIMS measurement to the entire sample would be an overestimation. Considering that the values for energy deposition vary across the sample and can be very high in selected areas, the overall energy in the ion pulse is consistent with the TNSA mechanism for laser to ion energy conversion in the few % range [2].

Based on the many SIMS profiles at different locations within the footprint of the beam with high concentrations at shallow depth and the resemblance of our enhancement to the diffusion of oxygen and carbon during laser annealing, we take the diffusion hypothesis to be plausible and have allowed for this in the analysis of the SIMS depth profiles. Based on the diffusivity of carbon and other elements in solid silicon, we assume the silicon must be at least above the melting temperature for substantial diffusion to occur on the relevant timescale. We calculated the duration the sample must remain above either the boiling or melting point in order to create the diffusion of at least 1 μm into the surface (Figure 3 (top)).

$$\Delta t_{melt}\,(1\mu m) \simeq \frac{L^2}{D_{melt}} = \frac{(1\cdot 10^{-4}\ cm^2)^2}{3.5\cdot 10^{-5}\ \frac{cm^2}{s}} = 3\cdot 10^{-4}\ s$$

$$\Delta t_{boil}(1\mu m) \simeq \frac{L^2}{D_{boil}} = \frac{(1\cdot 10^{-4}\ cm^2)^2}{2\cdot 10^{-4}\ \frac{cm^2}{s}} = 5\cdot 10^{-5}\ s$$

where D_{melt} and D_{boil} are diffusion coefficients extrapolated from measurements in Scharmann *et al.* and Narayan *et al.*, respectively [3,4]. Constrained by these published values for the diffusivity of carbon in silicon, both Δt_{melt} and Δt_{boil} are significantly longer than the 0.1 μs for which the sample is above the boiling points and the 1 μs for which the sample is above the melting point according to the finite-element heat diffusion simulation (Supplementary Figure 3, and Figure 4 in the main text), suggesting that there would not be enough time for surface carbons to diffuse 1 μm into the sample before it cools to below the melting point. Caveats to this suggestion include that the temperatures in Figure 3 are lower-limit estimates and that the diffusion coefficients might be extrapolated beyond their range of validity in order to calculate these estimates.

Notwithstanding the caveats and timescale issue above, we have calculated temperature profiles from the SIMS data by attributing the shallow-depth enhancement to diffusion of carbon from the surface. We therefore ignore the peaked diffusion component of the SIMS spectrum and make an exponential extrapolation to shallower depths based on the distribution for depths greater than ~2 μm (Figure 3, main text). The combination of the SIMS distribution at >2 μm and the extrapolation to shallow depth is taken to be the initial ion concentration profile in our 2D sample-heating model. The ion concentration profile is used to calculate an initial temperature profile.

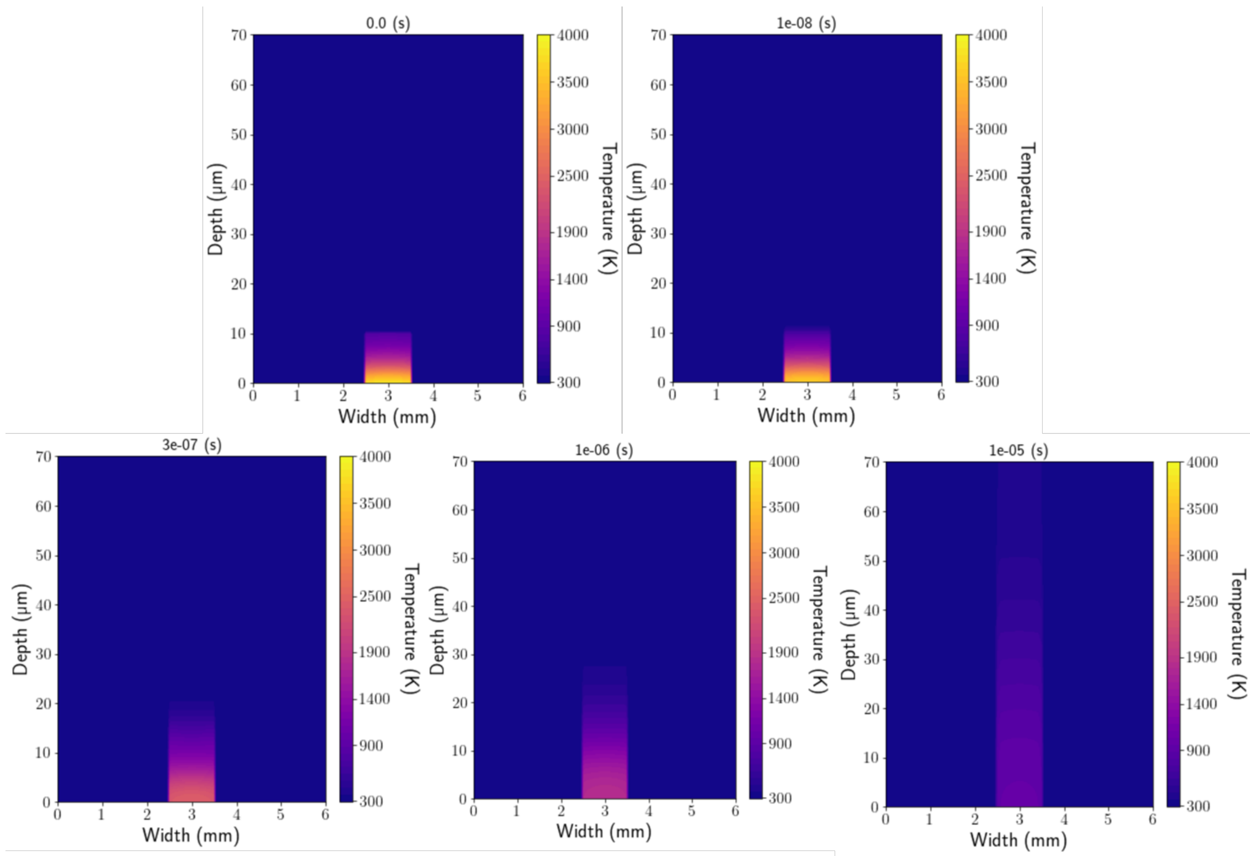

Supplementary Figure 3: **Frames of temperature evolution starting after a 10 ns ion pulse to 10 μs**. The sample cools to below the melting point after about 1 μs. The depth in this window is 70 μm and the beam spot is 1 mm wide in this example. Animation online: https://www.youtube.com/watch?v=Su1zf5hLi8c

Our simulation covers a region of 70 μm depth and 6 mm transverse width on our silicon sample. An initial gaussian transverse profile is assumed for the ion beam pulse (σ = 1.7 mm based on our NRA measurement) and the temperature vs depth at the center of the ion pulse is normalized to the SIMS-derived temperature profile. The gaussian is truncated at r = 0.5 mm to account for the ~1 mm beam diameter corresponding to the ~1 mm wide area where we observe surface exfoliation. Outside the 1 mm spot the temperature is set initially to 293 K. In order to simulate heat diffusion in the region over time, we solve the heat diffusion equation in the manner of Incropera *et al.* [5] (5.72):

$$\frac{1}{\alpha}\frac{\partial T}{\partial t} = \frac{\partial^2 T}{\partial x^2} + \frac{\partial^2 T}{\partial y^2}$$

where $\alpha = \frac{\kappa}{c_p \rho}$ is the thermal diffusivity. Similar to Table 5.3 in Incropera *et al.*, we produce the following three finite-difference equations for interior, side, and corner nodes, respectively, in our region of interest under adiabatic conditions

$$T_{m,n}^{p+1} = \frac{\alpha \Delta t}{\Delta x^2}[T_{m+1,n}^{p} + T_{m-1,n}^{p}] + \frac{\alpha \Delta t}{\Delta y^2}[T_{m,n+1}^{p} + T_{m,n-1}^{p}] + [1 - \frac{2\alpha \Delta t}{\Delta x^2} - \frac{2\alpha \Delta t}{\Delta y^2}]T_{m,n}^{p}$$

$$T_{m,n}^{p+1} = \frac{2\alpha \Delta t}{\Delta x^2}T_{m-1,n}^{p} + \frac{\alpha \Delta t}{\Delta y^2}[T_{m,n+1}^{p} + T_{m,n-1}^{p}] + [1 - \frac{2\alpha \Delta t}{\Delta x^2} - \frac{2\alpha \Delta t}{\Delta y^2}]T_{m,n}^{p}$$

$$T_{m,n}^{p+1} = \frac{2\alpha \Delta t}{\Delta x^2}T_{m-1,n}^{p} + \frac{2\alpha \Delta t}{\Delta y^2}T_{m,n-1}^{p} + [1 - \frac{2\alpha \Delta t}{\Delta x^2} - \frac{2\alpha \Delta t}{\Delta y^2}]T_{m,n}^{p}$$

where $T_{m,n}^{p}$ is the temperature of the node at the grid location (m, n) at the pth time step, Δt is the size of the time step, and Δx and Δy are the grid step sizes in x and y, respectively. Using a Python script, we recursively solve these equations to construct temperature profiles at times as early as 1 ns and as late as 1 ms after the initial heating of the sample. The depth profiles in Figure 4 (main text) were constructed by extracting the temperatures at the center of the beam pulse at the times of interest. The Python code was benchmarked against the commercial heat-transfer finite difference program FEHT and was found to be in good agreement [6].

In summary, our observed shallow-depth (top few µm) enhanced carbon concentration qualitatively resembles that of a diffusion process driven by sudden heating of silicon samples via laser annealing with short-pulse lasers [1]. We modeled the heat diffusion of the ion energy deposition and calculated the characteristic time that the sample remains in the molten phase where the diffusivity of carbon in silicon is higher. The difficulty with this interpretation is that the estimated time for the carbon to diffuse to a depth of $\sim$1 μm is longer than the cooling time. Yet, this depends greatly on the diffusion coefficients — for which there is considerable range in the literature — and the thermal conductivity of the samples [7].

Supplementary Note 4. Details on NRA

Silicon samples that had been exposed to 10 and 100 ion pulses were analyzed using NRA for the detection and depth profiling of ^{12}C, ^{14}N and ^{16}O isotopes through the $^{12}C(d,p_0)^{13}C$, $^{14}N(d,\alpha_1)^{12}C$ and $^{16}O(d,p_1)^{17}O$ nuclear reactions [8,9], respectively. The measurements were carried out with a 1.4 MeV deuteron beam, a beam diameter of 1 mm and a Passivated Implanted Planar Silicon (PIPS) Detector with an area of 300 mm^2 placed at the scattering angle θ=150°. A 13 µm thickness filter of aluminized Mylar was placed in front of the PIPS to avoid that elastically scattered deuterons reach the detector, which could saturate the electronic chain and produce pile-up. Reference samples consisting of thin layers of Si_3N_4/Si and Ta_2O_5/Ta with a known amount (±3%) of N and O were used to calibrate the NRA spectra, which were analyzed using the SIMNRA 6.0 code [8].

Supplementary Figure 4 shows an image of the surface of two samples after 10 and 100 shots, respectively, where it is apparent that the irradiated area was very inhomogeneous. A scan of 6 (10x

sample) and 8 (100x sample) NRA measurements along the horizontal direction was performed with 1 mm steps/point. An ion beam dose of 5 µC was accumulated for every point of analysis.

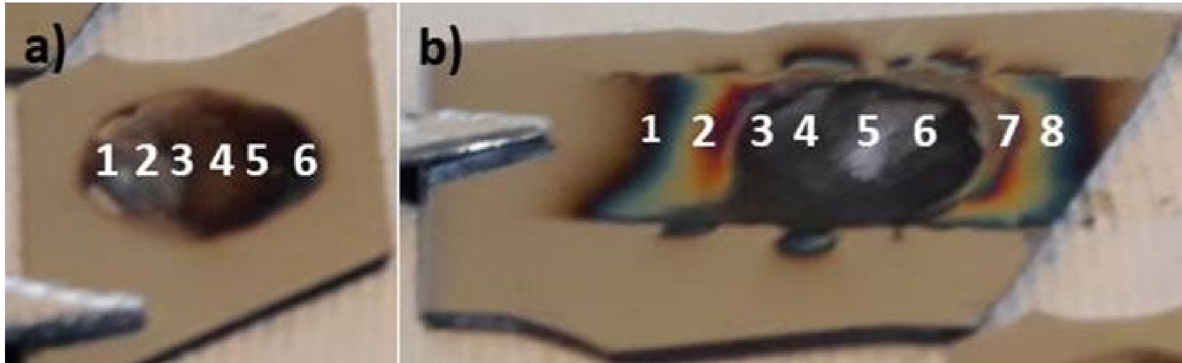

Supplementary Figure 4: **Optical images of samples after a series of laser-ion pulses**. (a) 10 ion pules and (b) 100 ion pulses with the corresponding impact points indicated where the NRA measurements have been performed. The measurement beam spot diameter was 1 mm at each measurement position.

Supplementary Figure 5 shows the NRA spectra obtained in an irradiated point (black spectrum) in comparison with the spectrum from an as received silicon sample (red spectrum). Except for the most intense signal, corresponding to the $^{12}C(d,p_0)^{13}C$ reaction, it is evident that there is strong overlap of the peaks coming from the ^{12}C, ^{14}N and ^{16}O isotopes with the signals produced with the ^{28}Si from the substrate that populate various excited states of ^{29}Si nuclei. Due to the unavailability of several cross sections data for the $^{28}Si(d,p_x)^{29}Si$ nuclear reactions, it was not possible to make a global fit of the spectra with the SIMNRA program. To overcome this difficulty and to be able to carry out the simulations, the spectrum from a pristine silicon target was subtracted from all measured spectra.

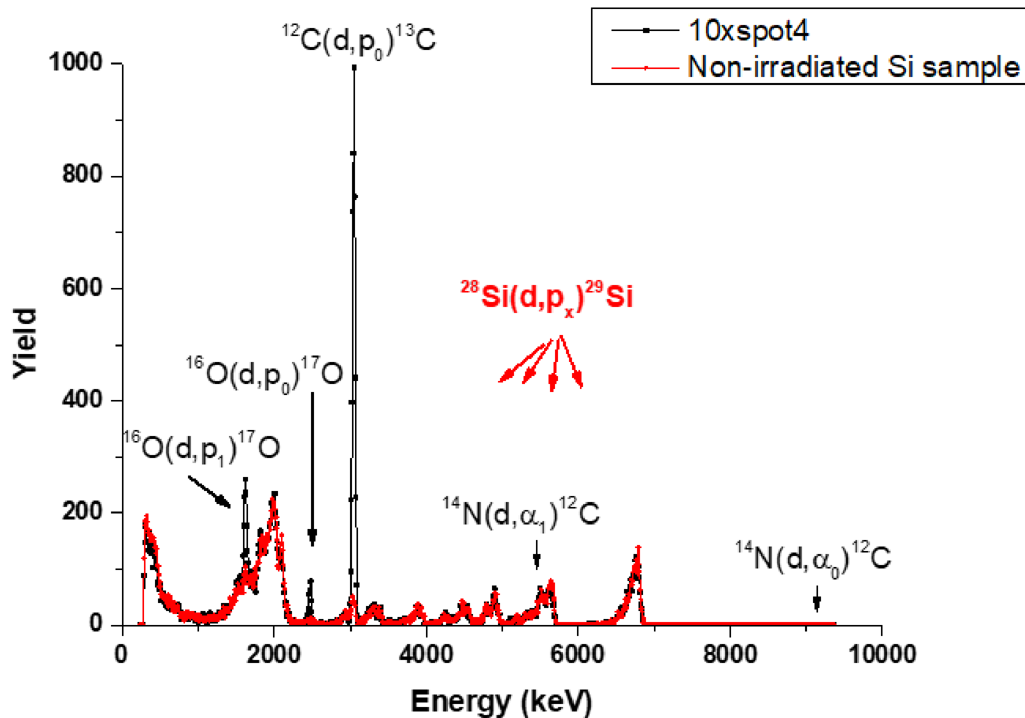

Supplementary Figure 5: **Examples of Nuclear reaction Analysis (NRA) spectra.** NRA spectrum measured in an irradiated spot (black signal) compared to spectrum from a pristine silicon sample (red signal).

Representative spectra obtained at different positions of the sample irradiated with 10 ion pulses, after subtraction of the background signal, are shown in Supplementary Figure 6. For all measured points we observe signals from carbon and oxygen atoms in the top 200 nm near the surface with respective fluences ranging between 75–250×10^{15} C cm^{-2} and 75–125×10^{15} O cm^{-2}. Only point 2 shows a depth profile for carbon, adding a fluence of 30×10^{15} C cm^{-2}, which extends to a depth of ~ 3.2 µm. For oxygen, it is not possible to know if the few counts that appear at energies lower than 1600 keV are due to a real oxygen profile or to an imperfect subtraction process of the Si signal. The nitrogen peaks (not shown) are very small and correspond to fluences between 9-27×10^{15} N cm^{-2}.

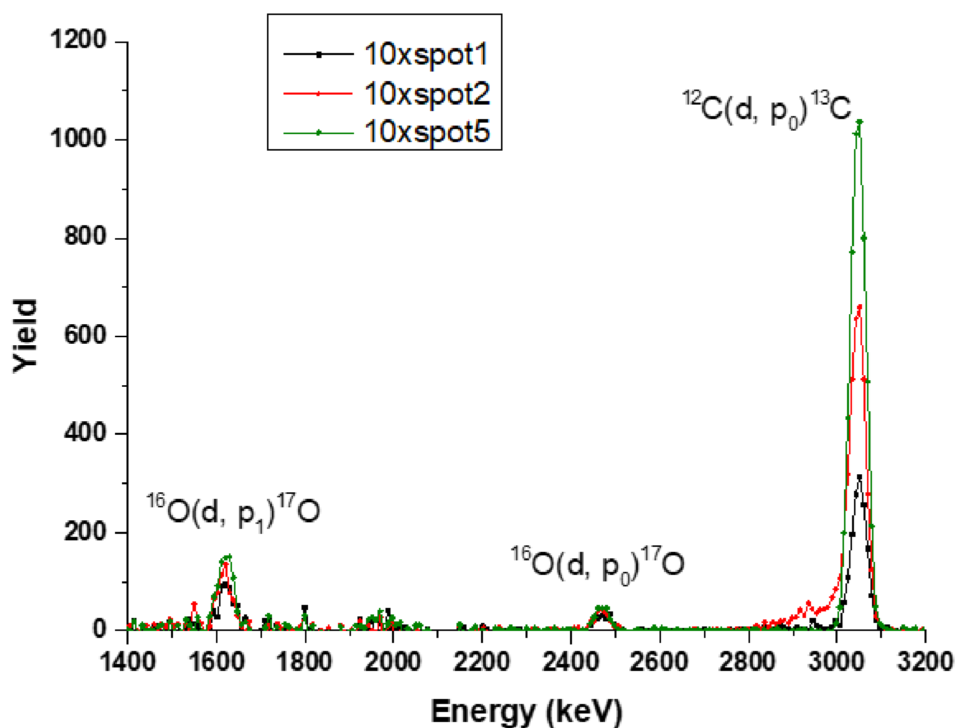

Supplementary Figure 6: **Nuclear reaction Analysis (NRA) spectra after subtraction of the silicon substrate signal.** NRA spectra for a series of positions across the 10x pulse sample corresponding to the areas in the image in Supplementary Figure 4 (a).

The NRA spectra acquired across a series of positions of the 100x pulse sample (Supplementary Figure 4 b), together with the SIMNRA simulation of the spectrum obtained at point 5, are displayed in Supplementary Figure 7. As expected from the optical image, the impurity content is very inhomogeneous, with values in the top 200 nm ranging between 245–1100×10^{15} C cm^{-2}, 75–260×10^{15} O cm^{-2} and 15–89×10^{15} N cm^{-2}, respectively.

a)

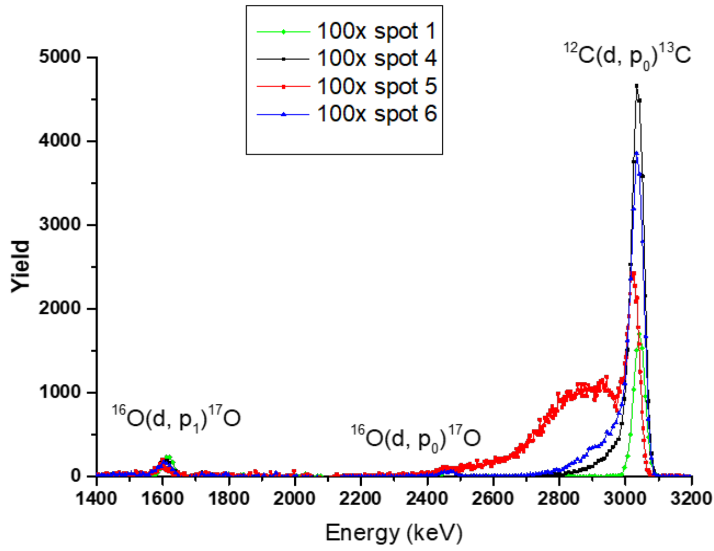

b)

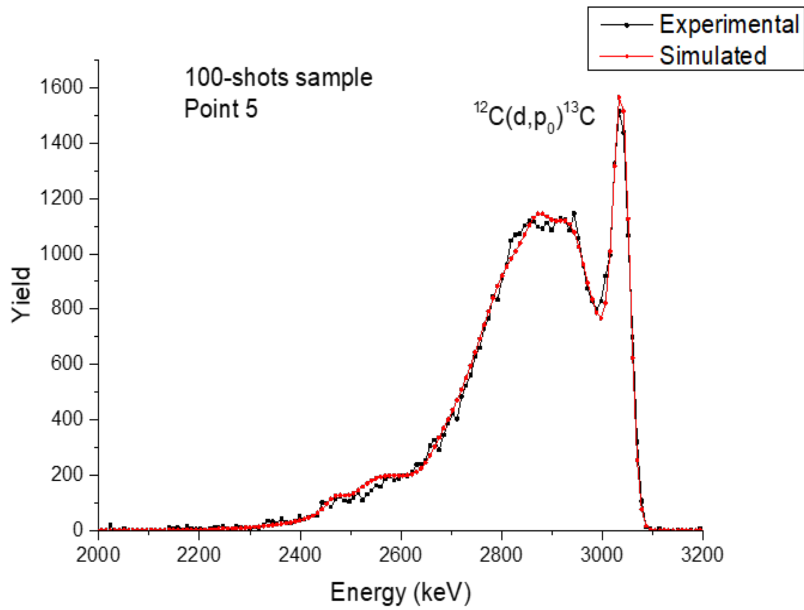

Supplementary Figure 7: **Nuclear reaction Analysis (NRA) spectra after 100 laser-ion pulses**. a): NRA spectra after subtraction of the silicon signal for a series of positions across the 100x pulse sample corresponding to the areas in the image in Supplementary Figure 4 b). b): Experimental and SIMNRA simulated spectra of the $^{12}C(d,p_0)^{13}C$ signal from spot 5.

For this sample, the deepest carbon atoms are highly localized (at point 5) where they reach a depth of ~7.5 +/- 1.5 µm. As discussed in the main text, a high fluence of low energy carbon ions, ~10^{16} cm^{-2} per pulse is implanted near the surface of the samples. Carbon at depths > 1 µm is from in-diffusion of carbon with a contribution of high energy ions from TNSA.

Supplementary Note 5. Details on Channeling RBS

In order to quantify the structure of silicon (111) crystals after a series of laser ion pulses, we conducted Rutherford Backscattering analysis in channeling direction (ch-RBS)[9, 10]. We used 2 MeV helium ions with a probe beam spot of 1 mm diameter. The energy resolution of the detector was 18 keV. The analysis geometry is shown in Supplementary Figure 8 together with typical spectra for silicon (111) samples that had been exposed to 1, 2, 10 and 100x laser ion pulses. Ch-RBS probes the top ~2 µm of the samples.

Ch-RBS is sensitive to the accumulation of radiation damage, such as point defects and dislocation loops, as well as surface structure changes from the impact of energetic ions on silicon crystals. We observe increasing backscattering yields in the channeling direction, increasing from the familiar very low yields in the pristine material for samples that received increasing numbers of pulses (Supplementary Figure 8). But the total accumulated disorder is much lower than expected for carbon ion irradiation with an energy deposition in the ~2 J/cm^2 range and carbon ion energies ranging from 0.1 to 8 MeV with fluences as shown in Figure 3 in the main text [10–12]. This is consistent with the high thermal budget from exposure to intense laser-ion pulses leading to point defect annealing and dislocation loop formation.

a)

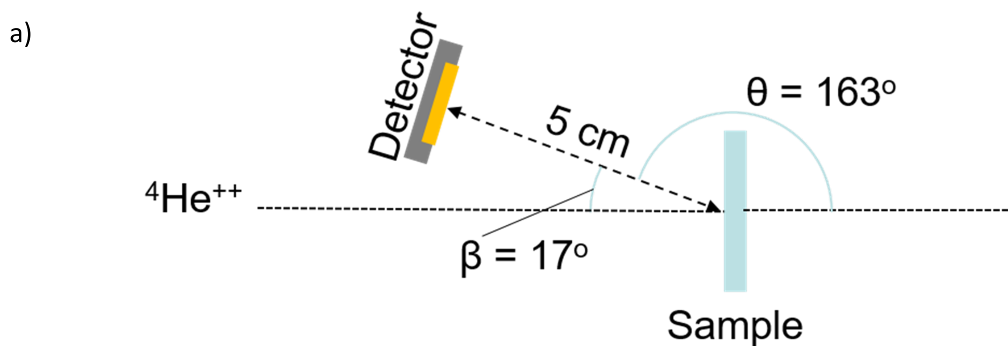

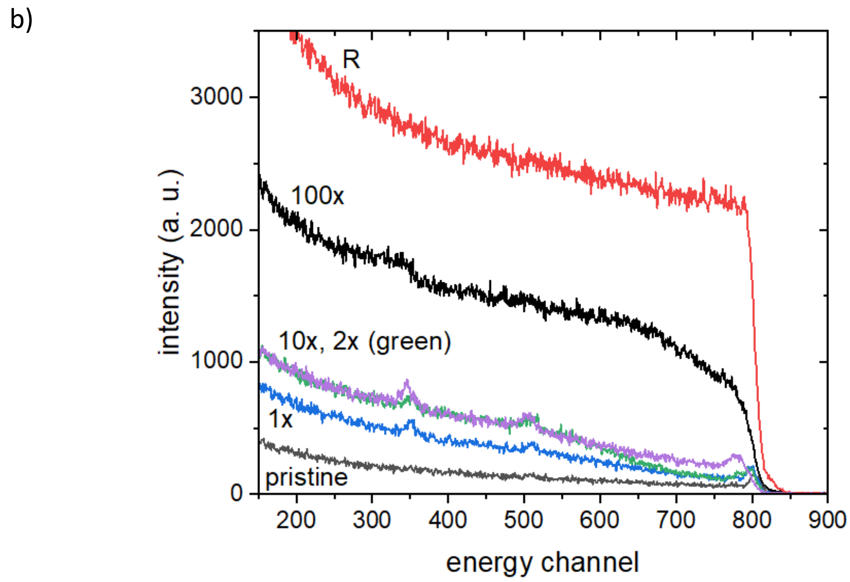

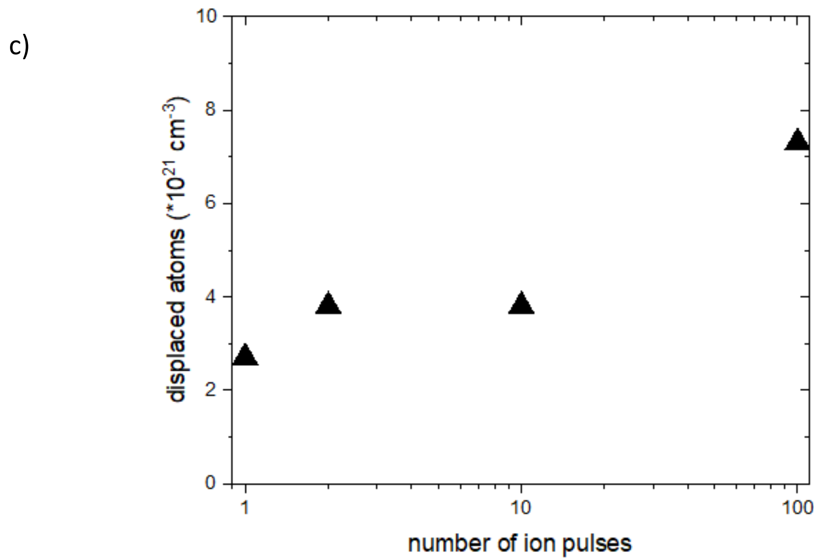

Supplementary Figure 8: **Setup and results from channeling-Rutherford Backscattering Spectrometry (ch-RBS)**. a): Schematic of the ch-RBS setup. b) Ch-RBS spectra for silicon (111) samples that had been exposed to 1, 2, 10 and 100x ion pulses, compared to a spectrum taken with random alignment (R, red), and from a pristine Si (111) sample. c) Concentration of displaced silicon atoms as a function of the number of laser ion pulses a silicon (111) had received.

Supplementary Note 6. Simulations of gaps between defect levels for the G-center and W-center

To understand the effect of excess carbon in proximity to a photon emitting defect, we performed calculations on the structures of G and W-centers embedded within a 3×3×3 silicon unit cell, with an additional interstitial carbon placed at one of the 106 possible tetrahedral sites within the supercell. The structures are fully relaxed and the energy splitting between the two defect levels within the silicon band gap are plotted vs the distance between the defect and an interstitial carbon atom (Supplementary Figure 9). When the carbon interstitial is close to the defect (< 5 Å), there is a dramatic effect on the defect levels. Greater separations (> 10 Å) correspond more closely to the expected separation between defects and stray interstitials at the typical observed concentrations below a few atomic % carbon in silicon. For these configurations, the G-center still has some spread in the gap energies of different configurations, but for the W-center the gaps are nearly identical, in line with the notion that the G-center is much more sensitive to local disorder than the W-center.

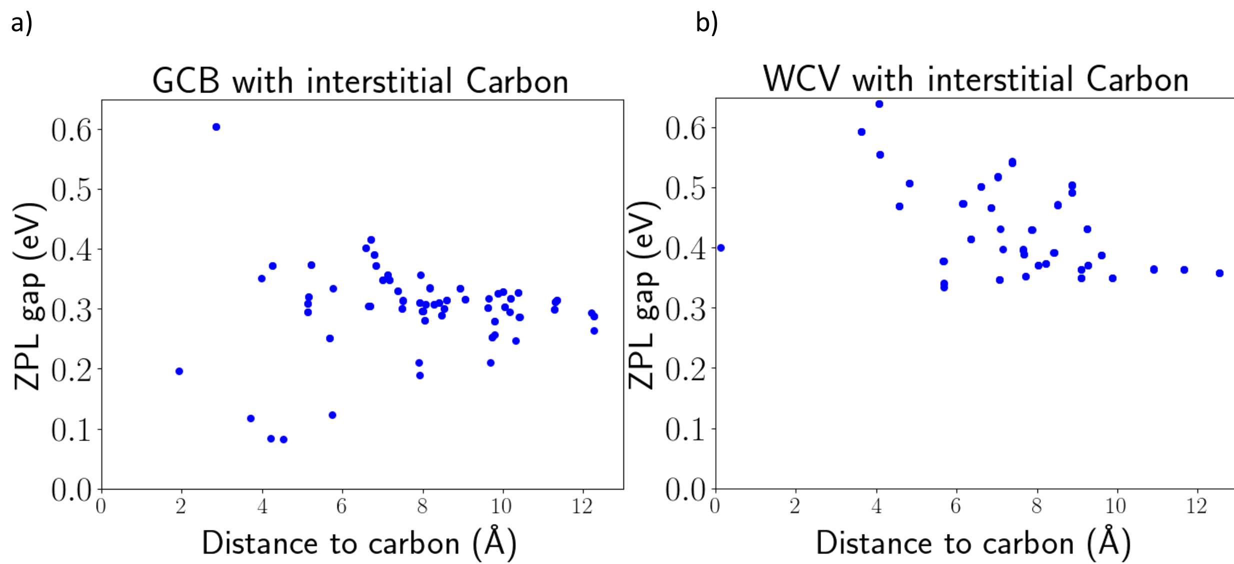

Supplementary Figure 9: **Simulations of gaps between defect levels for the G-center and W-center.** Zero-phonon line gap, calculated as the difference between lower and upper defect levels for G-centers (a) and W-centers (b) modulated by nearby interstitial carbon sites, plotted versus distance between the defect and interstitial carbon.

Supplementary References:

1. Monflier, R. et al. Investigation of oxygen penetration during UV nanosecond laser annealing of silicon at high energy densities. Applied Surface Science vol. 546, 149071 (2021).

2. Schreiber, J., Bolton, P. R. & Parodi, K. Invited Review Article: 'Hands-on' laser-driven ion acceleration: A primer for laser-driven source development and potential applications. Rev. Sci. Instrum. 87, 071101 (2016).

3. Scharmann, F., Maslarski, P., Lehmkuhl, D., Stauden, T. & Pezoldt, J. Evaluation of carbon surface diffusion on silicon by using surface phase transitions. Fourth International Workshop on Nondestructive Testing and Computer Simulations in Science and Engineering (2001) doi:10.1117/12.417645.

4. Narayan, J., Raghunathan, R., Chowdhury, R. & Jagannadham, K. Mechanism of combustion synthesis of silicon carbide. Journal of Applied Physics vol. 75, 7252 (1994).

5. Incropera, F. P. & DeWitt, D. P. Fundamentals of Heat and Mass Transfer. (John Wiley & Sons Incorporated, 1996).

6. Website. http://www.fchart.com/.

7. Barnard, J. J. & Schenkel, T. Modeling of intense pulsed ion beam heated masked targets for extreme materials characterization. Journal of Applied Physics 122, 195901 (2017).

8. Mayer, M. SIMNRA, a simulation program for the analysis of NRA, RBS and ERDA. in AIP Conference Proceedings (AIP, 1999). doi:10.1063/1.59188.

9. Wang, Y. & Nastasi, M. Handbook of Modern Ion Beam Materials Analysis. (Materials Research Society, 2010).

10. Feldman, L. C., Mayer, J. W. & Picraux, S. T. A. Materials Analysis by Ion Channeling: Submicron Crystallography. (Academic Press, 2012).

11. Nastasi, M. & Mayer, J. W. Ion Implantation and Synthesis of Materials. (Springer Science & Business Media, 2007).

12. Hodgson, R. T., Baglin, J. E. E., Pal, R., Neri, J. M. & Hammer, D. A. Ion beam annealing of semiconductors. Applied Physics Letters 37, 187 (1980).